${}^{3}_{\Lambda}\mathrm{H}$ and ${}^{3}_{\Lambda}\overline{\mathrm{H}}$ production and characterization in Cu + Cu collisions at $\sqrt{s_{NN}} = 200$ GeV

Feng-Xian Liu,[1,2] Gang Chen,[1,2,*] Zhi-Lei She,[1,2] Liang Zheng,[2] Yi-Long Xie,[2] Zi-Jian Dong,[2] Dai-Mei Zhou,[4] and Ben-Hao Sa[3,4]

[1]*Institute of Geophysics and Geomatics, China University of Geosciences, Wuhan 430074, China*
[2]*School of Mathematics and Physics, China University of Geosciences, Wuhan 430074, China*
[3]*China Institute of Atomic Energy, P.O. Box 275 (10), Beijing 102413, China*
[4]*Institute of Particle Physics, Central China Normal University, Wuhan 430079, China*

(Received 14 December 2018; published 14 March 2019)

Production of the (anti)hypertriton nuclei ${}^{3}_{\Lambda}\mathrm{H}$ and ${}^{3}_{\Lambda}\overline{\mathrm{H}}$ in Cu+Cu interactions at $\sqrt{s_{NN}} = 200$ GeV is studied in three centrality bins of 0–10%, 10–30%, and 30–60% using the dynamically constrained phase-space coalescence model together with PACIAE model simulations. They are compared with ${}^{3}\mathrm{H}$ (${}^{3}\overline{\mathrm{H}}$) and ${}^{3}\mathrm{He}$ (${}^{3}\overline{\mathrm{He}}$) nuclei. It is indicated by the study that the yields of light nuclei and hypernuclei increase rapidly from peripheral to central collisions while their antiparticle-to-particle ratios remain unchanged for different centrality bins. The strangeness population factor $S_3 = ({}^{3}_{\Lambda}\mathrm{H}/{}^{3}\mathrm{He})/(\Lambda/p)$ was found to be close to unity, and was compatible with the STAR data and theoretical model calculations, suggesting that the phase-space population of strange quarks is similar to the ones of light quarks and the creation of deconfined high-temperature quark matter in Cu+Cu collisions.

DOI: 10.1103/PhysRevC.99.034904

I. INTRODUCTION

The collisions of high-energy heavy ions can recreate conditions similar to that of the universe microseconds after the big bang, and produce abundant nuclei and antinuclei in this process [1]. Thus, high-energy heavy-ion collisions provide us a unique opportunity to study and understand the production and properties of nuclei and antinuclei under extreme energy conditions. Additionally, during the creation of deconfined quark gluon matter, the strange quark production is predicted to be largely enhanced due to thermal equilibrium, providing an important tool to produce light (anti)hypernuclei [2].

Since Danysz and Pniewski made the first observation of the hypernucleus in a nuclear emulsion cosmic ray detector in 1952 [3], a new field opened, called hypernuclear physics, extending the research scope of nuclear physics from the two-dimensional space of neutrons and protons to the three-dimensional space including the hyperons. Hypernuclei contain nucleons and hyperons (Λ, Ξ, Σ, Ω). Hyperons are usually unstable particles with at least one strange quark in their valence components.

The hypertriton (${}^{3}_{\Lambda}\mathrm{H}$) is the lightest hypernucleus; it contains a hyperon Λ and two nucleons (proton plus neutron). Since the first ${}^{3}_{\Lambda}\mathrm{H}$ was observed, several hypernuclei have been found; nevertheless, no antihypernucleus was discovered until the observation of the antihypertriton (${}^{3}_{\Lambda}\overline{\mathrm{H}}$) by the STAR Collaboration, using the Relativistic Heavy-Ion Collider (RHIC) at Brookhaven National Laboratory (BNL), in 2010 [4]. Hypernuclear physics is used to provide fascinating and fundamental information about not only the interaction between a hyperon and a baryon (YN) or a hyperon and a hyperon (YY), but also the influence caused by the hyperon motion when it enters a nucleus. These interactions are related to nuclear astrophysics and nuclear physics, such as the hyperon puzzle in studying the structure of neutron stars [5]. The inclusion of hyperons in microscopic theory results in too soft equation of state and too low maximum masses of neutron stars [6–9], which might be due to the current uncertainties on YN and YY interactions. The productions of hypernuclei and several antihypernuclei have been studied in heavy-ion collisions for many years, as mentioned earlier; for a review see Refs. [10–16] and references therein.

In this paper, the parton and hadron cascade model (PACIAE) [17] is used to simulate the production of (anti)nucleons ($p, \overline{p}, n, \overline{n}$) and (anti)hyperons ($\Lambda, \overline{\Lambda}$) in Cu+Cu collisions at $\sqrt{s_{NN}} = 200$ GeV, and to analyze their yields at mid-rapidity ($|\eta| < 0.5$). These yields are compared with experimental data from the STAR Collaboration [18–20] to fix the model parameters. Then, a dynamically constrained phase-space coalescence model (DCPC) [21–23] is used to study the production and properties of light (anti)nuclei clusters. We expect that their yields in Cu+Cu collisions may provide some information about the nature of ${}^{3}_{\Lambda}\mathrm{H}$ and ${}^{3}_{\Lambda}\overline{\mathrm{H}}$.

II. MODELS

The PACIAE [17] is based on PYTHIA 6.4 and was designed for various collision types ranging from $e^+ + e^-$, $p + p$, and $p + A$ to $A + A$ collisions. In general, PACIAE has four main physics stages consisting of the parton initiation, parton rescattering, hadronization, and hadron rescattering. The

*Corresponding author: chengang1@cug.edu.cn

TABLE I. The participants $\langle N_{\rm part}\rangle$ and yields of particles (p, $\overline{p}$, Λ, $\overline{\Lambda}$) in Cu+Cu collisions at $\sqrt{s_{NN}} = 200$ GeV for different centrality bins, compared with the STAR data [18–20].

Centrality		0–10%	10–30%	30–60%
$\langle N_{\rm part}\rangle$	PACIAE	103.4	67.9	28.4
	STAR	99.0 ± 1.5	64.2 ± 1.2	29.7 ± 0.7
p	PACIAE	5.73 ± 0.22	3.55 ± 0.23	1.42 ± 0.15
	STAR	$5.56 \pm 0.02 \pm 0.19$	$3.35 \pm 0.01 \pm 0.12$	$1.38 \pm 0.01 \pm 0.05$
$\overline{p}$	PACIAE	4.69 ± 0.18	2.91 ± 0.21	1.14 ± 0.11
	STAR	$4.54 \pm 0.02 \pm 0.13$	$2.79 \pm 0.01 \pm 0.08$	$1.16 \pm 0.01 \pm 0.03$
Λ	PACIAE	4.24 ± 0.13	2.59 ± 0.16	1.02 ± 0.12
	STAR	4.68 ± 0.45	2.67 ± 0.27	1.06 ± 0.11
$\overline{\Lambda}$	PACIAE	3.64 ± 0.11	2.26 ± 0.17	0.91 ± 0.10
	STAR	3.79 ± 0.37	2.18 ± 0.23	0.88 ± 0.09

parton initiation is the first stage, in which the nucleus-nucleus collision is decomposed into the nucleon-nucleon (NN) collisions according to the collision geometry and NN total cross section. The strings created in the NN collisions will break up into free partons leading to the formation of the deconfined quark gluon matter. After the parton initiation stage, the decomposed partons rescatter on each other based on the $2 \to 2$ LO-pQCD parton-parton cross sections [24]. Then, the hadronization proceeds through the Lund string fragmentation model [25] or the phenomenological coalescence model [17]. The final stage is the hadron rescattering process happening between the created hadrons until the hadronic freeze-out [17].

We calculate the production of light (anti)nuclei and (anti)hypernuclei with the DCPC model, which has been studied and used in several collision systems, such as Au+Au [22,23,26,27], Pb+Pb [28], and $p+p$ collisions [29]. We can obtain the yield of a single particle using the integral

$$Y_1 = \int_{H \leqslant E} \frac{d\vec{q}\, d\vec{p}}{h^3}, \tag{1}$$

where H and E present the Hamiltonian and energy of the particle, respectively. Then we can also know the yield of N particles calculated by the integral

$$Y_N = \int \cdots \int_{H \leqslant E} \frac{d\vec{q}_1 d\vec{p}_1 \ldots d\vec{q}_N d\vec{p}_N}{h^{3N}}. \tag{2}$$

This equation, however, has to meet the constraint conditions as follows:

$$m_0 \leqslant m_{inv} \leqslant m_0 + \Delta m, \tag{3}$$

$$q_{ij} \leqslant D_0 (i \neq j;\ j = 1, 2, \ldots, N), \tag{4}$$

where

$$m_{inv} = \left[\left(\sum_{i=1}^{N} E_i \right)^2 - \left(\sum_{i=1}^{N} p_i \right)^2 \right]^{1/2} \tag{5}$$

E_i and p_i $(i = 1, 2, \ldots, N)$ denote the energies and momenta of particles. m_0 and Δm respectively represent the rest mass and the allowed mass uncertainty. D_0 stands for the diameter of (anti)nuclei and (anti)hypernuclei, and $q_{ij} = |\vec{q}_i - \vec{q}_j|$ represents the vector distance between particle i and particle j. Here, the diameters are calculated by $D_0 = r_0 A^{1/3}$, so we choose $r_0 = 1.4, 1.5, 1.7$ and then get $D_0 = 2.02, 2.16, 2.45$ fm for ^{3}He ($^3\overline{\rm He}$), ^{3}H ($^3\overline{\rm H}$), $^3_\Lambda$H ($^3_{\overline{\Lambda}}\overline{\rm H}$) in the model, respectively [11,17,30,31].

III. RESULTS AND DISCUSSION

First we produce the final-state particles using the PACIAE model. In the PACIAE simulations, we assume that the hyperons heavier than Λ have already decayed before the creation of hypernuclei. The model parameters were fixed at the default values given in the PYTHIA model, except the K factor and the parameters parj(1), parj(2), and parj(3) were roughly fitted to the STAR data in Cu+Cu collisions at $\sqrt{s_{NN}} = 200$ GeV for different centrality bins of 0–10%, 10–30%, and 30–60%, where the transverse momentum spectra of final-state hadrons agree with STAR data. The yields of p, $\overline{p}$, Λ, and $\overline{\Lambda}$ are shown in Table I, where the yields of particles were calculated with $|\eta| < 0.1$ and $0.4 < p_T < 1.2$ GeV/c for p and $\overline{p}$, and $|\eta| < 0.5$ and $0 < p_T < 8$ GeV/c for Λ and $\overline{\Lambda}$. Here, parj(1) is the suppression of diquark-antidiquark pair production compared with the quark-antiquark pair production, parj(2) is the suppression of strange quark pair production compared with up (down) quark pair production, and parj(3) is the extra suppression of strange diquark production compared with the normal suppression of a strange quark. We choose parj(1) = 0.18, parj(2) = 0.43, and parj(3) = 0.40. The participants $\langle N_{\rm part}\rangle$ and corresponding experimental data [18–20] are also presented in Table I. It can be seen from Table I that the yields of particles (p, $\overline{p}$, Λ, and $\overline{\Lambda}$) all decrease rapidly with the increase of centrality, and the PACIAE model results agree with the STAR data within uncertainties.

Figure 1 shows the transverse momentum distributions of p and Λ (open symbols) at mid-rapidity for different centralities Cu+Cu collisions at $\sqrt{s_{NN}} = 200$ GeV calculated by the PACIAE model. The solid symbols in this figure are the experimental data taken from Refs. [18,19]. Obviously, one can see from Fig. 1 that the transverse momentum distributions of particles (p and Λ) calculated by the PACIAE model are compatible with the STAR data.

In the following, the nucleons and hyperons produced within PACIAE are used as input of the DCPC model. We

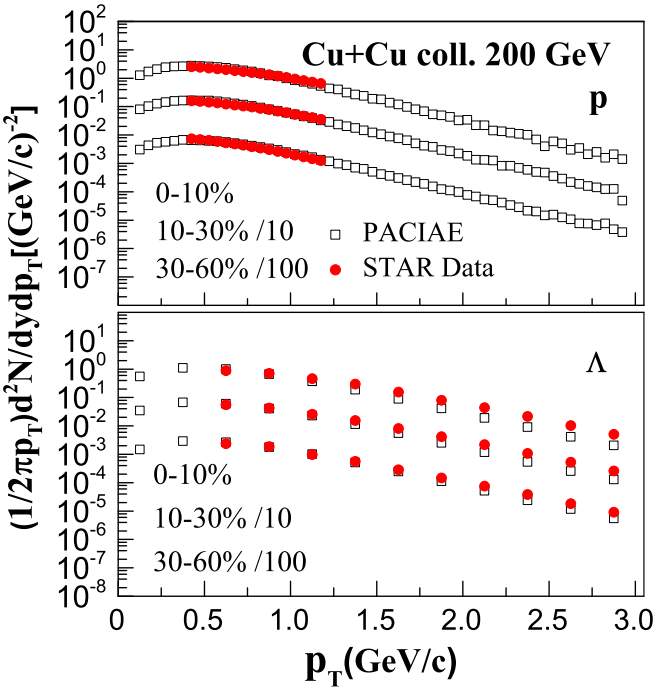

FIG. 1. The transverse momentum spectra of p (upper panel) and Λ (lower panel) in Cu+Cu collisions at $\sqrt{s_{NN}} = 200$ GeV for different centrality bins of 0–10%, 10–30%, and 30–60%. The open squares show the results of PACIAE model, and the filled circles show the STAR data [18,19].

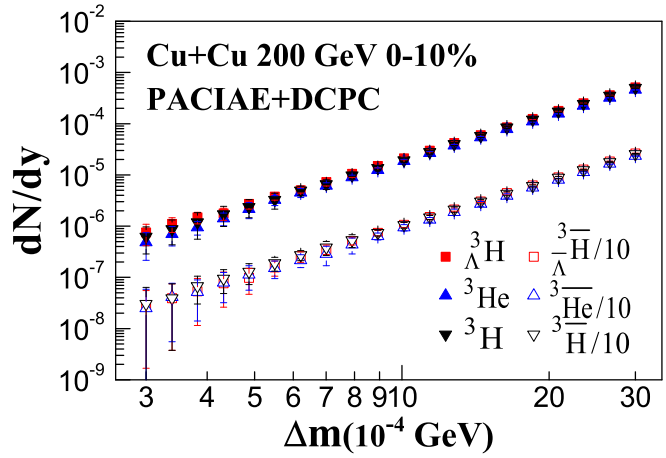

FIG. 2. Logarithmic distribution of the integrated yields dN/dy of nuclei $^3_\Lambda$H, ^{3}He, ^{3}H and their antinuclei, as a function of Δm with $|\eta| < 0.5$ and $0 < p_T < 6$ GeV/c. For clarity, data of nuclei and antinuclei are purposely separated by powers of 10.

generate 100 million minimum bias events for Cu+Cu collisions at $\sqrt{s_{NN}} = 200$ GeV with the PACIAE model. Then we obtain the integrated yields dN/dy for light nuclei and hypernuclei with $|\eta| < 0.5$ and $0 < p_T < 6$ GeV/c for the centrality bins of 0–10%, 10–30%, and 30–60%, respectively. Figure 2 compares their average yield per event at mid-rapidity for central (0–10%) Cu+Cu collisions at $\sqrt{s_{NN}} =$ 200 GeV with Δm varying from 0.3 to 3 MeV. We find that $\ln(dN/dy)$ increase linearly with $\ln \Delta m$. The behaviors of integrated yields dN/dy of light nuclei and hypernuclei are found to be similar.

Table II demonstrates the integrated yields dN/dy of $^3_\Lambda$H ($^3_\Lambda\overline{\text{H}}$), ^{3}H ($^3\overline{\text{H}}$), ^{3}He ($^3\overline{\text{He}}$) calculated by the PACIAE+DCPC model in 0–10%, 10–30% and 30–60% centrality classes Cu+Cu collisions of $\sqrt{s_{NN}} = 200$ GeV. Here the appropriate parameters Δm are fixed to be $\Delta m = 0.79$ MeV for $^3_\Lambda$H ($^3_\Lambda\overline{\text{H}}$) and $\Delta m = 0.89$ MeV for ^{3}H, $^3\overline{\text{H}}$, ^{3}He, and $^3\overline{\text{He}}$. The experimental data are taken from the STAR Collaboration [32]. Meanwhile, the PACIAE+DCPC model results are comparable to those of the experimental data within the current statistical errors.

In heavy-ion collisions, the production mechanism is generated through hadron coalescence due to final-state correlations between particles. The ratios of particle yields can be predicted by the coalescence model, and have been checked for various particle species. For instance, CERN Super Proton Synchrotron (SPS) data show that the production of nuclei in Pb+Pb collisions at $\sqrt{s_{NN}} = 17.3$ GeV is consistent with a coalescence picture [33].

Theoretically, the ratios of different (anti)nuclei and (anti)hypernuclei can be directly related to ratios of hadronic yields in the simple coalescence framework [34,35]. For example, if the $^3_\Lambda$H and $^3_\Lambda\overline{\text{H}}$ are formed by coalescence of $(p + n + \Lambda)$ and $(\overline{p} + \overline{n} + \overline{\Lambda})$, then the yield ratio of $^3_\Lambda\overline{\text{H}}/^3_\Lambda$H should be proportional to $(\overline{p}/p)(\overline{n}/n)(\overline{\Lambda}/\Lambda)$, and the other

TABLE II. The integrated yields dN/dy of the (anti)hypertriton as well as the (anti)triton and (anti)helium-3 are calculated by the PACIAE+DCPC model in Cu+Cu collisions of $\sqrt{s_{NN}} = 200$ GeV, compared with experimental data from STAR [32].

Nucleus type	STAR	PACIAE[a] (0–10%)	PACIAE[a] (10–30%)	PACIAE[a] (30–60%)
$^3_\Lambda$H (10^{-5})		1.05 ± 0.11	0.29 ± 0.04	0.022 ± 0.004
$^3_\Lambda\overline{\text{H}}$ (10^{-5})		0.51 ± 0.06	0.14 ± 0.02	0.012 ± 0.003
^{3}He (10^{-5})	1.29 ± 0.22	1.24 ± 0.12	0.37 ± 0.05	0.026 ± 0.005
$^3\overline{\text{He}}$ (10^{-5})	0.59 ± 0.09	0.61 ± 0.07	0.17 ± 0.03	0.014 ± 0.003
^{3}H (10^{-5})		1.38 ± 0.15	0.35 ± 0.05	0.029 ± 0.005
$^3\overline{\text{H}}$ (10^{-5})		0.74 ± 0.10	0.20 ± 0.03	0.016 ± 0.003

[a]Calculated with $\Delta m = 0.79$ MeV for $^3_\Lambda$H, $^3_\Lambda\overline{\text{H}}$ and $\Delta m = 0.89$ MeV for ^{3}He, $^3\overline{\text{He}}$, ^{3}H, $^3\overline{\text{H}}$.

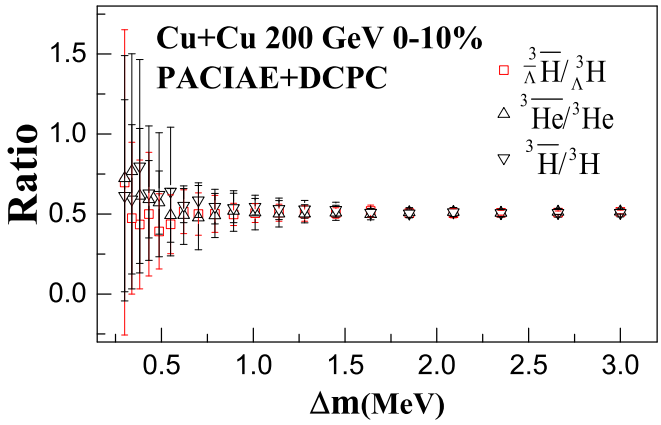

FIG. 3. The distribution of ratios $^3_\Lambda\overline{H}/^3_\Lambda H$, $^3\overline{He}/^3He$, and $^3\overline{H}/^3H$ versus the mass uncertainty (Δm) in Cu+Cu collisions at $\sqrt{s_{NN}} =$ 200 GeV($|\eta| < 0.5$ and $0 < p_T < 6$ GeV/c). Error bars are statistical only.

ratios are the same. The ratios can be written as

$$\frac{^3_\Lambda\overline{H}}{^3_\Lambda H} = \frac{\overline{pn}\overline{\Lambda}}{pn\Lambda} \simeq \left(\frac{\overline{p}}{p}\right)^2 \frac{\overline{\Lambda}}{\Lambda}, \tag{6}$$

and the mixed ratios as

$$\frac{^3_\Lambda H}{^3He} = \frac{pn\Lambda}{ppn} \simeq \frac{\Lambda}{p}, \tag{7}$$

$$\frac{^3_\Lambda H}{^3H} = \frac{pn\Lambda}{pnn} \simeq \frac{\Lambda}{p}, \tag{8}$$

$$\frac{^3_\Lambda\overline{H}}{^3\overline{He}} = \frac{\overline{pn}\overline{\Lambda}}{\overline{ppn}} \simeq \frac{\overline{\Lambda}}{\overline{p}}, \tag{9}$$

$$\frac{^3_\Lambda\overline{H}}{^3\overline{H}} = \frac{\overline{pn}\overline{\Lambda}}{\overline{pnn}} \simeq \frac{\overline{\Lambda}}{\overline{p}}. \tag{10}$$

The ratios $^3_\Lambda\overline{H}/^3_\Lambda H$, $^3\overline{He}/^3He$, and $^3\overline{H}/^3H$ calculated by the PACIAE+DCPC model with $|\eta| < 0.5$ and $0 < p_T < 6$ GeV/c, as a function of Δm, are shown in Fig. 3. It is clear that the ratios are close to 0.5 for almost all the mass uncertainty (Δm) range. The ratios of antinuclei to nuclei are independent of Δm, although their integrated yield dN/dy has a strong dependence on Δm as shown in Fig. 2. Since the $^3_\Lambda\overline{H}$ and $^3_\Lambda H$ are formed by coalescence of $(\overline{\Lambda} + \overline{p} + \overline{n})$ and $(\Lambda + p + n)$, the production ratio of $^3_\Lambda\overline{H}$ to $^3_\Lambda H$ should be proportional to $(\frac{\overline{p}}{p})^2\frac{\overline{\Lambda}}{\Lambda}$, as in Eq. (6). The latter value can be extracted from Table III, and the value obtained is 0.52 ± 0.10. The calculated $^3_\Lambda\overline{H}/^3_\Lambda H$ ratio is consistent with the interpretation that the $^3_\Lambda\overline{H}$ and $^3_\Lambda H$ are formed by coalescence of $(\overline{\Lambda} + \overline{p} + \overline{n})$ and $(\Lambda + p + n)$, respectively.

Table III represents ratios of antiparticles to corresponding particles ($\overline{p}/p$, $\overline{\Lambda}/\Lambda$, $^3_\Lambda\overline{H}/^3_\Lambda H$, $^3\overline{He}/^3He$, $^3\overline{H}/^3H$) and their mixed ratios (Λ/p, $\overline{\Lambda}/\overline{p}$, $^3_\Lambda H/^3He$, $^3_\Lambda\overline{H}/^3\overline{He}$, $^3_\Lambda H/^3H$, $^3_\Lambda\overline{H}/^3\overline{H}$) for centrality bins of 0–10%, 10–30%, and 30–60% in Cu+Cu collisions at $\sqrt{s_{NN}} = 200$ GeV, where $^3_\Lambda H$, $^3_\Lambda\overline{H}$ are calculated with $\Delta m = 0.79$ MeV and ^3He, $^3\overline{He}$, ^3H, $^3\overline{H}$ with $\Delta m =$ 0.89 MeV. The result with centrality bin 0–10% is drawn in Fig. 4. We can see from Table III that the yield ratios of $\overline{p}/p$, $\overline{\Lambda}/\Lambda$, $^3_\Lambda\overline{H}/^3_\Lambda H$, $^3\overline{He}/^3He$, $^3\overline{H}/^3H$ and their mixed ratios Λ/p, $\overline{\Lambda}/\overline{p}$, $^3_\Lambda H/^3He$, $^3_\Lambda\overline{H}/^3\overline{He}$, $^3_\Lambda H/^3H$, $^3_\Lambda\overline{H}/^3\overline{H}$ are all independent of the centrality bin, although their yields decrease rapidly with centrality as shown in Tables I and II. The ratios of the (anti)hypertriton to (anti)nuclei ($^3_\Lambda H/^3He$, $^3_\Lambda\overline{H}/^3\overline{He}$, $^3_\Lambda H/^3H$, $^3_\Lambda\overline{H}/^3\overline{H}$) are less than 1, which means that the yield of the (anti)hypertriton is less than that of (anti)nuclei.

Table III and Fig. 4 show that the ratios of the (anti)hypernuclei to (anti)nuclei ($^3_\Lambda H/^3He$, $^3_\Lambda\overline{H}/^3\overline{He}$, $^3_\Lambda H/^3H$,

TABLE III. The (anti)nucleus ratios from the PACIAE+DCPC model in Cu+Cu collisions at $\sqrt{s_{NN}} = 200$ GeV for three different centrality classes. The top section of the table shows the three ratios of antinucleus to nucleus, followed by the mixed ratios of (anti)nucleus to (anti)nucleus. The ratios between proton, antiproton, hyperon, and antihyperon are shown at the bottom. In the top two sections, STAR data are taken from Au+Au collisions at $\sqrt{s_{NN}} = 200$ GeV [4], and, at the bottom, STAR data are taken from Cu+Cu collisions at $\sqrt{s_{NN}} = 200$ GeV [18,19].

Ratio	STAR	PACIAE (0–10%)	PACIAE (10–30%)	PACIAE (30–60%)
$^3_\Lambda\overline{H}/^3_\Lambda H$	$0.49 \pm 0.18 \pm 0.07$	0.50 ± 0.06	0.49 ± 0.07	0.54 ± 0.12
$^3\overline{He}/^3He$	$0.45 \pm 0.02 \pm 0.04$	0.51 ± 0.06	0.46 ± 0.06	0.53 ± 0.11
$^3\overline{H}/^3H$		0.54 ± 0.07	0.58 ± 0.09	0.56 ± 0.12
$^3_\Lambda\overline{H}/^3\overline{He}$	$0.89 \pm 0.28 \pm 0.13$	0.84 ± 0.10	0.83 ± 0.12	0.86 ± 0.21
$^3_\Lambda H/^3He$	$0.82 \pm 0.16 \pm 0.12$	0.85 ± 0.08	0.80 ± 0.12	0.85 ± 0.20
$^3_\Lambda\overline{H}/^3\overline{H}$		0.70 ± 0.09	0.71 ± 0.11	0.76 ± 0.19
$^3_\Lambda H/^3H$		0.77 ± 0.11	0.82 ± 0.14	0.75 ± 0.18
$\overline{p}/p$	0.80 ± 0.04	0.81 ± 0.05	0.82 ± 0.08	0.80 ± 0.11
$\overline{\Lambda}/\Lambda$	0.82 ± 0.12	0.86 ± 0.04	0.87 ± 0.09	0.88 ± 0.15
Λ/p	0.84 ± 0.09	0.74 ± 0.04	0.73 ± 0.07	0.72 ± 0.12
$\overline{\Lambda}/\overline{p}$	0.83 ± 0.08	0.78 ± 0.05	0.78 ± 0.08	0.80 ± 0.12

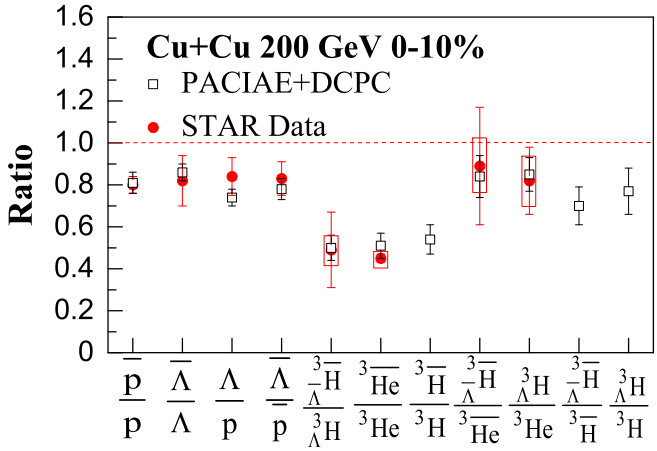

FIG. 4. The ratios $(\overline{p}/p$, $\overline{\Lambda}/\Lambda$, $^3_{\overline{\Lambda}}\overline{\text{H}}/^3_\Lambda\text{H}$, $^3\overline{\text{He}}/^3\text{He}$, $^3\overline{\text{H}}/^3\text{H})$ and $(p/\Lambda$, $\overline{\Lambda}/\overline{p}$, $^3_\Lambda\text{H}/^3\text{He}$, $^3_{\overline{\Lambda}}\overline{\text{H}}/^3\overline{\text{He}}$, $^3_\Lambda\text{H}/^3\text{H}$, $^3_{\overline{\Lambda}}\overline{\text{H}}/^3\overline{\text{H}})$ determined by the PACIAE+DCPC model analysis (open squares) for matter and antimatter compared with STAR results (filled circles) [4]. Here, statistical and systematic errors are represented by error bars and error boxes, respectively.

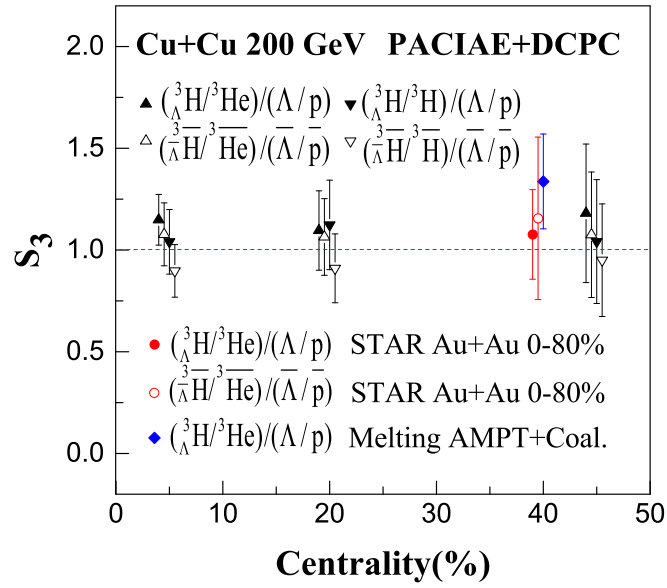

FIG. 5. The S_3 $(\overline{S}_3)$ ratio as a function of the centrality in Cu+Cu collisions at $\sqrt{s_{NN}} = 200$ GeV. For comparison, the data from STAR Au+Au 0–80% collisions at $\sqrt{s_{NN}} = 200$ GeV [4] and minimum bias Au+Au collisions from the melting AMPT plus coalescence model calculation [42] are shown here. Statistical uncertainties are represented by bars.

$^3_{\overline{\Lambda}}\overline{\text{H}}/^3\overline{\text{H}}$), as Eqs. (6)–(10) predict, are compatible to the ratio of hyperon to proton within uncertainties. The simulation results in our model are found to be in agreement with the experimental data from STAR (0–80% centrality) Au+Au collisions at $\sqrt{s_{NN}} = 200$ GeV [4,18,19]. Furthermore, the model predictions of $^3\overline{\text{H}}/^3\text{H}$, $^3_\Lambda\text{H}/^3\text{H}$, and $^3_{\overline{\Lambda}}\overline{\text{H}}/^3\overline{\text{H}}$ are also presented in Fig. 4.

The strangeness population factor for light nuclei $S_3 = (^3_\Lambda\text{H}/^3\text{He})/(\Lambda/p)$, in a naive coalescence model, should be a value near unity, as Ref. [11] shows. The ratio is sensitive to the local baryon-strangeness correlation [36–41], hence it can provide a possible chance to study the nature of matter created in the collision [42,43]. The S_3 $(\overline{S}_3)$ values obtained by the PACIAE+DCPC model for different centrality bins of 0–10%, 10–30%, and 30–60% are shown in Fig. 5 and Table IV. These values are compared with a theoretical model [42] and the data from STAR [4].

The model used for the comparison is the string melting of AMPT (A Multi-Phase Transport Model for Relativistic Heavy Ion Collisions) [44] plus coalescence described in Ref. [42]. The present results in Cu+Cu collisions at $\sqrt{s_{NN}} =$ 200 GeV show values of S_3 $(\overline{S}_3)$ close to unity, indicating that the phase-space populations for strange and light quarks are similar, implying that high-temperature deconfined quarks can be formed in Cu+Cu collisions. These results are also consistent with the STAR experiment [4] and the AMPT with string melting plus coalescence model in Au+Au collisions at $\sqrt{s_{NN}} = 200$ GeV within uncertainties.

IV. CONCLUSION

In the paper, we have used the PACIAE model to simulate Cu+Cu collisions at a center-of-mass energy $\sqrt{s_{NN}} =$ 200 GeV. The obtained yields of final state particles p, $\overline{p}$, n, $\overline{n}$, Λ, and $\overline{\Lambda}$ within the PACIAE model are in very good agreement with experimental data from STAR. The p, $\overline{p}$, n, $\overline{n}$, Λ, and $\overline{\Lambda}$ are used as input for the DCPC model to construct $^3_\Lambda\text{H}$, $^3_{\overline{\Lambda}}\overline{\text{H}}$, ^3He, $^3\overline{\text{He}}$, ^3H, and $^3\overline{\text{H}}$ clusters through coalescence. A

TABLE IV. S_3 ratio for nucleus and antinucleus calculated by the PACIAE+DCPC model in Cu+Cu collisions of $\sqrt{s_{NN}} = 200$ GeV for three different centrality classes. The data for comparison are taken from STAR Au+Au 0–80% collisions at 200 GeV [4] and from minimum bias Au+Au collisions using the melting AMPT plus coalescence model calculations [42].

	Centrality	$(^3_\Lambda\text{H}/^3\text{He})/(\Lambda/p)$	$(^3_{\overline{\Lambda}}\overline{\text{H}}/^3\overline{\text{He}})/(\overline{\Lambda}/\overline{p})$	$(^3_\Lambda\text{H}/^3\text{H})/(\Lambda/p)$	$(^3_{\overline{\Lambda}}\overline{\text{H}}/^3\overline{\text{H}})/(\overline{\Lambda}/\overline{p})$
PACIAE+DCPC	0–10%	1.15 ± 0.12	1.08 ± 0.15	1.04 ± 0.16	0.90 ± 0.13
	10–30%	1.10 ± 0.20	1.06 ± 0.19	1.12 ± 0.22	0.91 ± 0.17
	30–60%	1.18 ± 0.34	1.08 ± 0.31	1.04 ± 0.30	0.95 ± 0.27
STAR	0–80%	1.08 ± 0.22	1.16 ± 0.40		
Melting AMPT+Coal.	0–80%	1.34 ± 0.23			

comparison between ${}^{3}_{\Lambda}\mathrm{H}$, ${}^{3}_{\Lambda}\overline{\mathrm{H}}$ and ${}^{3}\mathrm{He}$, ${}^{3}\overline{\mathrm{He}}$, ${}^{3}\mathrm{H}$, ${}^{3}\overline{\mathrm{H}}$ in Cu+Cu collisions at $\sqrt{s_{NN}} = 200$ GeV for three centrality classes (0–10%, 10–30%, and 30–60%) has been presented.

The results show that yields of ${}^{3}_{\Lambda}\mathrm{H}$, ${}^{3}_{\Lambda}\overline{\mathrm{H}}$, ${}^{3}\mathrm{He}$, ${}^{3}\overline{\mathrm{He}}$, ${}^{3}\mathrm{H}$, and ${}^{3}\overline{\mathrm{H}}$ decrease rapidly with the increase of centrality bins, but their yield ratios are independent of centrality, which is consistent with the STAR experimental data. The ratios of the (anti)hypertriton to (anti)nuclei (${}^{3}_{\Lambda}\mathrm{H}/{}^{3}\mathrm{He}$, ${}^{3}_{\Lambda}\overline{\mathrm{H}}/{}^{3}\overline{\mathrm{He}}$, ${}^{3}_{\Lambda}\mathrm{H}/{}^{3}\mathrm{H}$, ${}^{3}_{\Lambda}\overline{\mathrm{H}}/{}^{3}\overline{\mathrm{H}}$) are less than 1, which means that the yield of the (anti)hypertriton is less than that of (anti)nuclei. The strangeness population factor $S_3 = ({}^{3}_{\Lambda}\mathrm{H}/{}^{3}\mathrm{He})/(\Lambda/p)$ for matter and antimatter with tritium and helium-3 is calculated to be close to unity, which is compatible with the STAR data and the AMPT with string melting plus coalescence model, suggesting that the phase-space population of strange quarks is similar to the ones of light quarks and supports the generation of high-temperature matter of deconfined quarks. The yields and yield ratios of ${}^{3}_{\Lambda}\mathrm{H}$ (${}^{3}_{\Lambda}\overline{\mathrm{H}}$), ${}^{3}\mathrm{H}$ (${}^{3}\overline{\mathrm{H}}$), and ${}^{3}\mathrm{He}$ (${}^{3}\overline{\mathrm{He}}$) in Cu+Cu collisions at $\sqrt{s_{NN}} = 200$ GeV, were first predicted with the theoretical model.

ACKNOWLEDGMENTS

Financial support from NSFC (11475149,11775094) is acknowledged, as well as support by the high-performance computing platform of China University of Geosciences. The authors thank Huan Chen and Wei Dai for helpful discussions.

[1] H. Agakishiev *et al.* (STAR collaboration), Nature (London) **473**, 353 (2011).
[2] A. Andronic, P. Braun-Munzinger, J. Stachel, and H. Stocker, Phys. Lett. B **697**, 203 (2011).
[3] M. Danysz and J. Pniewski, Philos. Mag. **44**, 348 (1953).
[4] B. I. Abelev *et al.*, Science **328**, 58 (2010).
[5] I. Vidaña, Proc. R. Soc. London A **474**, 20180145 (2018).
[6] F. Weber, R. Negreiros, P. Rosenfield, and A. T. i. Cuadrat, in *7th Conference on Quark Confinement and the Hadron Spectrum - QCHS7*, 2–7 September 2006, Ponta Delgada, Acores (Portugal), edited by J. Emilio *et al.*, AIP Conf. Proc. No. 892 (AIP, New York, 2007), p. 515.
[7] H. J. Schulze and T. Rijken, Phys. Rev. C **84**, 035801 (2011).
[8] H. Dapo, B. J. Schaefer, and J. Wambach, Phys. Rev. C **81**, 035803 (2010).
[9] D. Lonardoni, F. Pederiva, and S. Gandolfi, J. Phys.: Conf. Ser. **529**, 012012 (2014).
[10] P. Braun-Munzinger and J. Stachel, J. Phys. G **21**, L17 (1995).
[11] T. A. Armstrong *et al.* (E864 Collaboration), Phys. Rev. C **70**, 024902 (2004).
[12] Y. G. Ma, J. H. Chen, and L. Xue, Front. Phys. **7**, 637 (2012).
[13] Y. G. Ma, J. Phys.: Conf. Ser. **420**, 012036 (2013).
[14] Y. G. Ma, EPJ Web Conf. **66**, 04020 (2014).
[15] P. Liu, J. H. Chen, Y. G. Ma, and S. Zhang, Nucl. Sci. Technol. **28**, 55 (2017).
[16] J. H. Chen, D. Keane, Y. G. Ma *et al.*, Phys. Rep. **760**, 1 (2018).
[17] B. H. Sa, D. M. Zhou, Y. L. Yan *et al.*, Comput. Phys. Commun. **183**, 333 (2012).
[18] M. M. Aggarwal *et al.* (STAR Collaboration), Phys. Rev. C **83**, 034910 (2011).
[19] G. Agakishiev *et al.* (STAR Collaboration), Phys. Rev. Lett. **108**, 072301 (2012).
[20] B. I. Abelev *et al.* (STAR Collaboration), Phys. Lett. B **673**, 183 (2009).
[21] Y.-L. Yan, G. Chen, X.-M. Li, D.-M. Zhou, M.-J. Wang, S.-Y. Hu, L. Ye, and B.-H. Sa, Phys. Rev. C **85**, 024907 (2012).
[22] G. Chen, Y.-L. Yan, D.-S. Li, D.-M. Zhou, M.-J. Wang, B.-G. Dong, and B.-H. Sa, Phys. Rev. C **86**, 054910 (2012).
[23] G. Chen, H. Chen, J. Wu, D. S. Li, and M. J. Wang, Phys. Rev. C **88**, 034908 (2013).
[24] B. L. Combridge, J. Kripfgang, and J. Ranft, Phys. Lett. B **70**, 234 (1977).
[25] T. Sjöstrand, S. Mrenna, and P. Skands, J. High Energy Phys. 05 (2006) 026.
[26] G. Chen, H. Chen, M. J. Wang *et al.*, J. Phys. G: Nucl. Part. Phys. **41**, 115102 (2014).
[27] Z.-J. Dong, Q. Y. Wang, G. Chen *et al.*, Eur. Phys. J. A **54**, 144 (2018).
[28] Z. L. She, G. Chen *et al.*, Eur. Phys. J. A **52**, 93 (2016).
[29] P. Sittiketkorn, K. Tomuang *et al.*, Phys. Rev. C **96**, 064002 (2017).
[30] S. Hamieh, K. Redlich, and A. Tounsi, Phys. Lett. B **486**, 61 (2000).
[31] H. Nemura, Y. Suzuki, Y. Fujiwara, and C. Nakamoto, Prog. Theor. Phys. **103**, 929 (2000).
[32] J. Zhou, Light (anti-)nuclei production in the STAR experiment at RHIC, Ph.D. thesis, Rice University, 2009 (unpublished).
[33] R. Arsenescu *et al.* (NA52 Collaboration), New J. Phys. **5**, 150 (2003).
[34] J. Cleymans, S. Kabana, I. Kraus, H. Oeschler, K. Redlich, and N. Sharma, Phys. Rev. C **84**, 054916 (2011).
[35] L. Xue, Y. G. Ma, J. H. Chen, and S. Zhang, Phys. Rev. C **85**, 064912 (2012).
[36] V. Koch, A. Majumder, and J. Randrup, Phys. Rev. Lett. **95**, 182301 (2005).
[37] A. Majumder and B. Müller, Phys. Rev. C **74**, 054901 (2006).
[38] M. Cheng, P. Hegde, C. Jung, F. Karsch, O. Kaczmarek *et al.*, Phys. Rev. D **79**, 074505 (2009).
[39] J. Adams *et al.*, Nucl. Phys. A **757**, 102 (2005).
[40] P. Braun-Munzinger and J. Stachel, Nature (London) **448**, 302 (2007).
[41] R. V. Gavai and S. Gupta, Phys. Rev. D **73**, 014004 (2006).
[42] S. Zhang, J. Chen, H. Crawford, D. Keane, Y. Ma *et al.*, Phys. Lett. B **684**, 224 (2010).
[43] H. Sato and K. Yazaki, Phys. Lett. B **98**, 153 (1981).
[44] Z. W. Lin, C. M. Ko, B. A. Li, B. Zhang, and S. Pal, Phys. Rev. C **72**, 064901 (2005).